Environmental Science & Technology

pubs.acs.org/est

Article

Molecular Binding of Eu^{III}/Cm^{III} by *Stenotrophomonas bentonitica* and Its Impact on the Safety of Future Geodisposal of Radioactive Waste

Miguel A. Ruiz-Fresneda,* Margarita Lopez-Fernandez,* Marcos F. Martinez-Moreno, Andrea Cherkouk, Yon Ju-Nam, Jesus J. Ojeda, Henry Moll, and Mohamed L. Merroun

Cite This: *Environ. Sci. Technol.* 2020, 54, 15180−15190

Read Online

ACCESS | Metrics & More | Article Recommendations | Supporting Information

ABSTRACT: Microbial communities occurring in reference materials for artificial barriers (e.g., bentonites) in future deep geological repositories of radioactive waste can influence the migration behavior of radionuclides such as curium (Cm^{III}). This study investigates the molecular interactions between Cm^{III} and its inactive analogue europium (Eu^{III}) with the indigenous bentonite bacterium *Stenotrophomonas bentonitica* at environmentally relevant concentrations. Potentiometric studies showed a remarkably high concentration of phosphates at the bacterial cell wall compared to other bacteria, revealing the great potential of *S. bentonitica* for metal binding. Infrared spectroscopy (ATR-FTIR) and X-ray photoelectron spectroscopy (XPS) confirmed the role of phosphates and carboxylate groups from the cell envelope in the bioassociation of Eu^{III}. Additionally, time-resolved laser-induced fluorescence spectroscopy (TRLFS) identified phosphoryl and carboxyl groups from bacterial envelopes, among other released complexing agents, to be involved in the Eu^{III} and Cm^{III} coordination. The ability of this bacterium to form a biofilm at the surface of bentonites allows them to immobilize trivalent lanthanide and actinides in the environment.

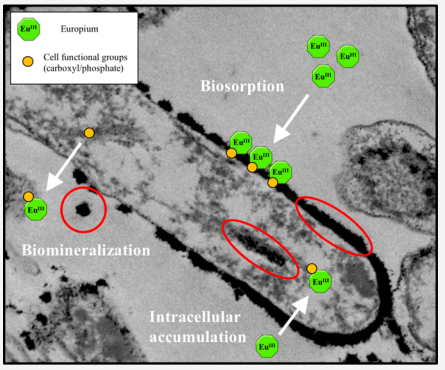

KEYWORDS: *europium, curium, bacterial speciation, mobility, geodisposal*

1. INTRODUCTION

The safe disposal of radioactive waste is crucial to ensure the safety of future generations, as well as for the biosphere. The implementation of deep geological repositories (DGRs) is planned in the near future for the disposal of high level (HLW) and long-lived radioactive wastes, which are the most hazardous because they contain larger radionuclide concentrations and longer lived radionuclides.[1] The DGR is a multibarrier system to deposit radioactive waste, mainly generated by the nuclear industry. A DGR option is to encapsulate the nuclear waste in metal containers (steel, iron, copper, etc.) surrounded by compacted bentonites, considered as geotechnical barriers, and emplace them in a stable geological formation at about 500−1000 m depth.[2] A high microbial diversity in bentonite clay formations from Almeria (Spain), considered as reference material of engineered barriers for repositories, has been previously reported.[3,4] Several studies have evidenced the impact of microbial processes on the corrosion of metal containers (steel, iron, copper, etc.), which could lead to the release of radionuclides to the surrounding environment.[5] Microbial processes also seem to play a crucial role controlling the speciation and mobility of radionuclides present in radioactive wastes, such as uranium (U) and curium (Cm).[3,4,6] Therefore, understanding the migration behavior and the environmental fate of radionuclides influenced by microorganisms will be essential for the risk assessment of repositories. Cm is a highly toxic radionuclide as indicated by the high α activity of some isotopes, such as ^{247}Cm (half-life: 1.6×10^7 years) and ^{248}Cm (half-life: 3.5×10^6 years) present in nuclear spent fuel.[7,8] Cm is a representative of trivalent actinides (An^{III}), which exhibits excellent luminescence properties that make it suitable for direct speciation studies at environmentally relevant metal concentration.[9] Similarly, europium (Eu) has been studied as an inactive analogue of An^{III}, also providing excellent luminescence properties.[10]

Among other mechanisms, microbes can interact with actinides and lanthanides through biosorption at cell surfaces.[11] A number of functional groups (e.g., carboxyl, phosphoryl) on microbial surfaces have been described to be effective for actinide complexation.[12,13] Cm^{III} and Eu^{III} form

Received: April 17, 2020
Revised: October 19, 2020
Accepted: November 5, 2020
Published: November 13, 2020

strong complexes with phosphoryl and carboxyl sites of the bacterial cell wall of *Sporomusa* sp. MT-2.99 and *Pseudomonas fluorescens*.[12,14] Recently, Yeasts and Archaea have also been investigated for their ability to complex An^{III} (e.g., Cm) and trivalent lanthanides (Ln^{III}) (e.g., Eu) through carboxyl and phosphate groups.[15,16] In addition, biofilm formation by microorganisms has to be considered, as it can lead to the immobilization of bioabsorbed radionuclides within the DGR system and consequently can affect their integrity.

Because cell surfaces play a major role in the complexation of Cm^{III} and Eu^{III}, different spectroscopic and microscopic techniques can be used to investigate the contribution of functional groups and the corresponding mechanisms involved in the biosorption of these elements. Attenuated total reflection−Fourier transform infrared (ATR-FTIR) spectroscopy, X-ray photoelectron spectroscopy (XPS), and time-resolved laser-induced fluorescence spectroscopy (TRLFS) are useful spectroscopic tools to determine the chemical speciation of these elements at environmentally relevant conditions. Potentiometric titrations have been used to determine types and abundance of active metal binding sites at the cell surface.[17,18] While a multidisciplinary approach combining different microscopic, spectroscopic, and potentiometric titration-based methods is usually applied to investigate the interactions of U, as hexavalent actinide, with microbes,[13,19] the microbial interactions with Cm and Eu have only covered the use of TRLFS and potentiometric techniques.[12,14]

Spanish bentonite clays (Almeria, Spain) have shown to be excellent and suitable reference material of engineered barriers for DGRs due to their physicochemical properties (low permeability, plasticity, high swelling pressure, thermal conductivity, etc.).[4] From these clays, *Stenotrophomonas bentonitica* has been isolated and well characterized[20] and shown to influence the chemical speciation and mobility of other elements present in radioactive waste such as selenite (Se^{IV}) and U^{VI}.[4,21] However, the interactions between Eu^{III}/Cm^{III} and *S. bentonitica* have never been described previously. For all mentioned above, the use of this strain as a model bentonite bacterial strain to investigate the impact of bentonite microbial population in the speciation of radionuclides within the concept of DGR is novel and could provide interesting results with regard to the biological, chemical, and physical analyses that are currently in progress to evaluate the DGR safety.

The present work studies the effect of *S. bentonitica* on the environmental fate of Eu^{III} and Cm^{III} under aerobic and anaerobic conditions, analogous to those expected in the geodisposal of radioactive waste. For this purpose, a combination of spectroscopic (ATR-FTIR, XPS, TRLFS) and microscopic (STEM-HAADF: scanning transmission electron microscopy-high angle annular dark field) techniques have been employed.

This study will provide new insights on the influence of bentonite bacterial isolates in the immobilization of An^{III} within the concept of radioactive waste disposal and will be useful to compare with other studies using elements such as Se and U. The safety of the DGR system has been well studied from a geological, chemical, and physical point of view, but not many studies have been conducted on the influence of microbiology. Therefore, this work is crucial to better understand how microbes can affect the safety of the disposal of such residues, which is a major environmental problem nowadays.

2. MATERIALS AND METHODS

Experimental procedures related to preparation of Eu^{III} and Cm^{III} stock solutions, potentiometric titration of cell surfaces of *S. bentonitica* treated with Eu^{III}, Eu^{III} biosorption experiments, TRLFS experimental setup, and STEM-HAADF analysis are provided in Supporting Information. Due to the hazardous nature and difficult handling of Cm^{III}, proper safety precautions and methodologies were employed in this study.

2.1. Bacterial Strain and Growth Conditions. The bacterial strain used was isolated from bentonite clay formations recovered from Almeria (Spain)[4] and was recently described as a novel species named *Stenotrophomonas bentonitica* BII-R7^T.[22] The cells were grown aerobically in Luria−Bertani (LB) broth medium (tryptone 10 g/L, yeast extract 5 g/L, and NaCl 10 g/L, pH 7.0 ± 0.2) at 28 °C under agitation (180 rpm).

2.2. Attenuated Total Reflection−Fourier Transform Infrared (ATR-FTIR) Spectroscopy. *S. bentonitica* cells were suspended in a 30 μM Eu^{III} chloride solution ($EuCl_3 \cdot 6H_2O$) under aerobic conditions at pH 6. After 48 h, the samples were collected by centrifugation (2700*g*; 10 min) and washed with 0.1 M $NaClO_4$. Finally, the samples were lyophilized according to standard protocols.[17,23] Bacterial cells without addition of Eu^{III} were employed as controls.

ATR-FTIR measurements were performed on a PerkinElmer Spectrum Two spectrometer, equipped with an ATR accessory, consisting of a diamond crystal at a fixed angle of 45°. Thirty two scans with spectral resolution 4 cm^{-1} and wavenumber range from 4000 to 400 cm^{-1} were collected for each sample. All measurements were performed in triplicate.

2.3. X-ray Photoelectron Spectroscopy (XPS). Eu^{III}-treated cells of *S. bentonitica* were prepared as described in section above (section 2.2). The obtained powder was mounted on standard sample studs using double-sided adhesive tape. Nontreated cells were prepared and used as controls. XPS measurements were made on a Kratos Supra photoelectron spectrometer at 10 kV and 20 mA using a monochromatic Al Kα X-ray source (1486.6 eV). The takeoff angle was fixed at 90°. On each sample the data were collected from three randomly selected locations, and the area corresponding to each acquisition was 400 μm in diameter. Each analysis consisted of a wide survey scan (pass energy 160 eV, 1.0 eV step size) and high-resolution scan (pass energy 20 eV, 0.1 eV step size) for component speciation. All experiments were conducted in triplicate. The binding energies of the peaks were determined using the C_{1s} peak at 284.5 eV. The software CasaXPS 2.3.17 was used to fit the XPS spectra peaks.[24]

2.4. Time-Resolved Laser-Induced Fluorescence Spectroscopy (TRLFS) Analyses. TRLFS measurements were performed to determine Eu^{III}/Cm^{III} species involved in interactions with the bacterial cells. Cells of *S. bentonitica* were brought into contact with 30 μM Eu^{III} both aerobically and anaerobically and with 0.3 μM Cm^{III} anaerobically and collected as indicated in section 1.3 of Supporting Information. The inactivity and hence easy handling of Eu^{III} allowed the TRLFS studies under both respiring conditions. The Cm^{III} experiments were performed anaerobically in a glovebox to exclude carbonate complexation of Cm^{III} and for radiation protection issues. The obtained pellets were washed and subsequently resuspended in 5 mL of 0.1 M $NaClO_4$ for analysis by TRLFS. For Eu^{III}, the pH was kept constant at 6,

https://dx.doi.org/10.1021/acs.est.0c02418
Environ. Sci. Technol. 2020, 54, 15180−15190

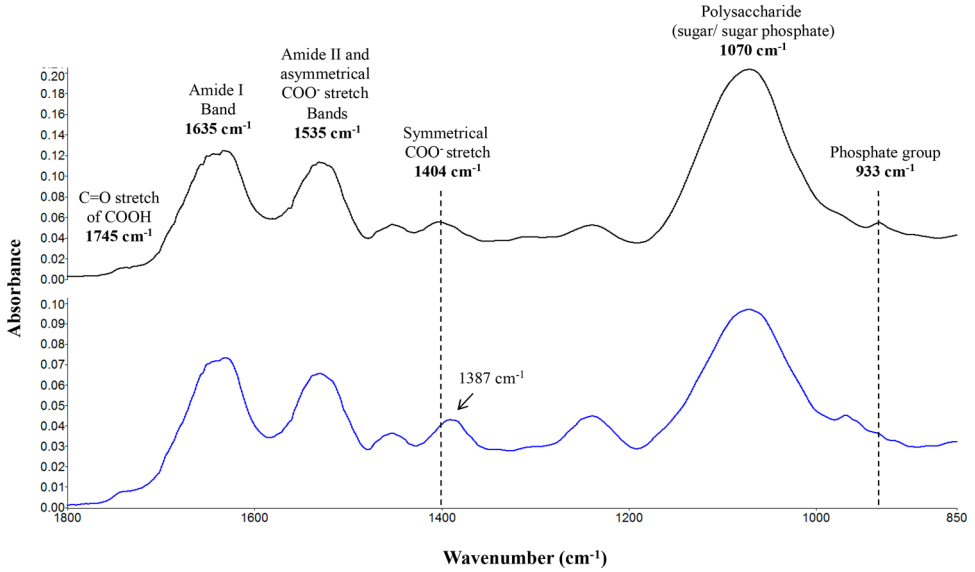

Figure 1. Comparison between the ATR-FTIR spectra for *S. bentonitica* cell suspensions in 0.1 M $NaClO_4$ (electrolyte) solution only (top, in black color) and in 30 μM Eu^{III} solution + electrolyte (bottom, in blue color) after 48 h.

while varying the incubation time (1, 24, and 48 h). For Cm^{III}, a pH-dependent spectroscopic titration (pH 2.33 to 8.04) was carried out.

3. RESULTS AND DISCUSSION

3.1. Potentiometric Titration Studies. The potentiometric titrations curves of *S. bentonitica* BII-R7 before and after Eu^{III} exposure are presented in Figure S1. The concentration of deprotonated sites is standardized per mass of dry biomass (mol g^{-1}) and calculated according to Fein et al.[25] To calculate the acidity constants and the total concentration of each binding site, data from the titrations curves were fitted using ProtoFit 2.1 rev1,[26] using a nonelectrostatic model (NEM). It has been demonstrated that electrostatic treatments, such as diffuse layer and triple layer electrostatic models to titration data, greatly overpredict the effect of ionic strength on bacterial surface protonation reactions, resulting in poorer fits and more variability in stability constants than nonelectrostatic models.[27,28]

The titrated bacterial suspensions exhibited a protonation−deprotonation behavior over the whole pH range studied (Figure S1). The shape of the titration curves obtained suggested the presence of functional groups with close acid−base pK_a values, showing that although some small variability could be perceived in each set of the same bacterial sample, essentially reproducible results were obtained (the variation between the titration curves was below 6% of $[H^+]_{exchanged}$ between pH 3.5 and 10.0). Although a small hysteresis could be observed between acid and base titrations at the same ionic strength, results from reverse titrations did not vary strongly and suggested a reversible proton adsorption/desorption reaction.

Table S1 summarizes the pK_a values for *S. bentonitica* before and after Eu^{III} exposure. The calculated values were 4.97 ± 0.08 and 4.78 ± 0.06 for pK_1, 6.88 ± 0.02 and 6.75 ± 0.13 for pK_2, and 9.43 ± 0.02 and 9.48 ± 0.11 for pK_3. The obtained pK_a values are representative of carboxylic groups for pK_1, phosphate groups for pK_2, and amine and hydroxyl groups for pK_3.[17,18,25,29−32]

The existence of pH zero proton charge (pH_{zpc}) indicated that *S. bentonitica* developed a positive net charge at low pH values, indicating the presence of at least one positively ionizing, plausibly amino group. Models which only include negatively ionizing groups such as carboxyl, phosphoryl, and hydroxyl groups could not develop a net positive charge at low pH.[33] The pH_{zpc} around 5.7 also indicated that the cells were negatively charged at neutral pH = 7 and that electrostatic attraction with positive-charged mineral surfaces or metals is favorable.

The surface site densities obtained using ProtoFit are also presented in Table S1. The pK_a values for bacterial samples with and without Eu^{III} were comparable, indicating similar concentrations of the active functional groups on the cell wall. One exception was found, the concentrations corresponding to phosphate groups (C_2) was significantly lower for *S. bentonitica* cells exposed to Eu^{III}. This could suggest a strong affinity of Eu^{III} for phosphate sites, making them inaccessible to the protonation/deprotonation reaction. The considerably high concentration of phosphate groups at the surface of *S. bentonitica* (10.78 ± 0.31 × 10^{-4} mol/g) compared with other bacterial species such as *Sporomusa* sp. MT-2.99 (5.30 ± 0.8 × 10^{-4} mol/g), *Sphingomonas* sp. S15−S1 (3.16 ± 0.56 × 10^{-4} mol/g), or *B. sphaericus* JG-7B (2.19 ± 0.25 × 10^{-4} mol/g)[12,34] (Table S1) pointed out the potentially high metal-binding ability of *S. bentonitica*.

The results of potentiometric titration experiments indicated that the cell surface groups capable for metal binding sites could involve carboxyl groups (pK around 3−5), phosphate groups (pK around 6−7), and hydroxyl and amine groups (pK > 8). These findings are in agreement with previous studies on bacterial surfaces.[17,35,36] Liu et al.[36] demonstrated the role of carboxyl, phosphoryl, and amino functional groups of *Synechococcus* sp. PCC 7002 cells as metal surface ligands by means of potentiometric titrations. In the case of Eu^{III} and Cm^{III}, their sorption on the cell envelope of *Sporomusa* sp. MT-2.99, *B. subtilis*, and *P. fluorescens* can be due to their coordination with carboxyl and phosphate groups.[12,14,37,38] Consequently, phosphate and carboxyl groups of *S. bentonitica* might be expected to be involved in the binding of Eu^{III}.

https://dx.doi.org/10.1021/acs.est.0c02418
Environ. Sci. Technol. 2020, 54, 15180−15190

However, the potentiometric results only showed phosphate groups as the main potential binding sites in the pH range studied due to their high surface concentration. It is probable that the extent of the carboxyl group involvement in the Eu^{III} binding is either too small to be detected by titration methods, or the sorption/desorption of Eu^{III} by the carboxylic groups is reversible at low pH (possible exchange between Eu(III) and protons at low pH for the carboxylate groups).

3.2. Eu^{III} Removal Capacity of *S. bentonitica* over Time. These studies were carried out to estimate the Eu^{III} removal capacity of *S. bentonitica* with increasing time under aerobic and anaerobic conditions. The maximum amount of Eu^{III} removal was 12.9 ± 0.11 mg of Eu/g of dry biomass after 96 h of aerobic incubation (Figure S2). This amount corresponds to a 54 ± 0.44% of Eu^{III} removed from the total amount of Eu in the solution. Higher values were obtained by Bader et al. (2019)[16] in their bioassociation kinetics studies with the halophilic archaeon *Halobacterium noricense* DSM15987^T by using the same Eu^{III} initial concentration (30 μM). They found that around 73% of Eu^{III} was removed after 1 week of incubation. Under anaerobic conditions, the maximum amount of Eu^{III} removal was 6.06 ± 0.25 mg of Eu/g of dry biomass after 18 h incubation (Figure S2), which corresponds to a 31.2 ± 1.3% of Eu^{III} removal. The Eu^{III} removal improved by increasing contact time of incubation until equilibrium was attained under both conditions. However, these results clearly showed that *S. bentonitica* cells have a higher removal capacity under aerobic conditions. This could be a consequence of the more stressful anoxic conditions, probably affecting the bacterial interaction process.

These results suggested that the interaction was mediated not only by biosorption, because this mechanism is generally defined as a quick process occurring up to a few hours.[39] More specifically, the Eu^{III} removal studies showed that time-dependent Eu interaction with the cells could be a biphasic process. First, a rapid phase where 12.5 ± 0.73 and 13.9 ± 1% of Eu^{III} removal was achieved (aerobically and anaerobically, respectively) within the first 2 h (Figure S2). This fast phase is usually associated with metabolic-independent biosorption mechanisms. Second, a slow phase seems to occur, where the Eu^{III} accumulation process seems to reach equilibrium after 24 h. This phase could be controlled by metabolically dependent interaction mechanisms such as intracellular accumulation or bioprecipitation, among others.

3.3. Characterization of Eu^{III}–*S. bentonitica* Interactions Using ATR-FTIR. Figure 1 shows the ATR-FTIR spectra obtained from *S. bentonitica* after 48 h incubation with 30 μM Eu^{III} solution. The observed infrared bands confirmed the presence of proteins, lipids, polysaccharides, and polyphosphate groups. The functional groups assigned to the infrared bands and the corresponding frequencies for the bacterial cells are summarized in Table S2.

The region between 3000 and 2800 cm^{-1} exhibited the typical C−H stretching vibrations (ν_{C-H}) corresponding to the CH_3 and $>CH_2$ functional groups present in the fatty acids and lipids, and the O−H stretching band (ν_{O-H}) corresponding to the presence of hydroxyl groups in bacterial cells. Complementary information could be found at the region between 1800 and 750 cm^{-1}, where vibrations of C−H, $>CH_2$, and CH_3 groups, amides, carbonyl groups, and polysaccharides were observed. The peaks observed at 1308 and 1455 cm^{-1} could be attributed to the bending of CH_3 and $>CH_2$ of proteins (δ_{CH2}, δ_{CH3}), and the signals at 1635 and 1535 cm^{-1} corresponded to the amide I and II bands, respectively. The amide I band was due to the stretching C=O ($\nu_{C=O}$) of amides associated with proteins, and the amide II band was actually a combination of bending N−H (δ_{N-H}) of amides and contributions from stretching C−N (ν_{C-N}) groups. The peak at 1455 cm^{-1} also concealed the amine III group. The peak around 1404 cm^{-1} was due to the symmetric stretching C−O of carboxylate groups ($\nu_{sym\ COO^-}$), and the peak corresponding to the asymmetric stretching vibration ($\nu_{asym\ COO^-}$) was concealed by the amide II band at 1535 cm^{-1}. A small shoulder around 1745 cm^{-1} was a combination of two peaks: a signal corresponding to the vibrational C=O stretching ($\nu_{C=O}$) of carboxylic acids at 1747 cm^{-1} and another peak corresponding to the stretching C=O of ester functional groups from membrane lipids and fatty acids at 1730 cm^{-1}.[17,30,31,40] The double bond stretching of >P=O of general phosphoryl groups and phosphodiester of nucleic acids could be observed at 1240 cm^{-1}. The stretching of P=O groups of polyphosphate products, nucleic acid phosphodiesters, and phosphorylated proteins can be found around 1070 cm^{-1}, and the peak at 933 cm^{-1} showed the asymmetric O−P−O stretching modes.[30,31,40]

The ATR-FTIR spectra showed a shift in the band attributed to symmetric stretching of carboxylate groups (around 1404 cm^{-1}) to lower frequencies, when compared to the spectra of the cells in background electrolyte (Figure 1). Extensive studies made on metal complexes of carboxylic acids have established an empirical correlation between the position of the symmetric stretching ($\nu_{sym\ COO^-}$) and asymmetric stretching ($\nu_{asym\ COO}$) of carboxylate groups and the difference in frequency between them ($\Delta\nu$). The values of $\Delta\nu$ descend in the follow order: $\Delta\nu_{unidentate} > \Delta\nu_{brinding} \sim \Delta\nu_{free\ ionic} > \Delta\nu_{chelate(bidentate)}$.[41−44] Chu et al.[41] and Deacon and Phillips,[44] after careful examinations of IR spectra of many acetates with known X-ray crystal structures, arrived at the conclusion that (i) for unidentates complexes, $\Delta\nu > 200$ cm^{-1} and the position of $\nu_{sym\ COO^-}$ is generally shifted to lower frequencies; (ii) for bidentate chelating complexes, $\Delta\nu < 100$ cm^{-1} and the position of $\nu_{sym\ COO^-}$ is shifted to higher frequencies, whereas $\nu_{asym\ COO^-}$ is shifted to lower frequencies; and (iii) for bidentate bridging complexes, $\Delta\nu \sim 160$ cm^{-1} and the position of $\nu_{sym\ COO^-}$ and $\nu_{asym\ COO^-}$ can shift in either direction.[41] The symmetric stretching ($\nu_{sym\ COO^-}$) band for *S. bentonitica* in contact with Eu^{III} shifted to lower frequencies by ∼15 cm^{-1}, but, as can be observed in Figure 1 and Table S2, the asymmetric stretching (ν_{asym} COO^-) of carboxylate groups was hidden by the amide II band, and therefore it is difficult to determine if there was a shift in this band to higher or lower frequencies. Based purely on the position of $\nu_{sym\ COO^-}$ shifting to lower frequencies, the carboxyl functional groups could form unidentate complexes with the Eu^{III} metals. If the asymmetric stretching ($\nu_{asym\ COO^-}$) of carboxylate groups (hidden by the amide II band) did not shift, then $\Delta\nu$ would be around 150 cm^{-1}, suggesting that the carboxyl functional groups arising from the macromolecules of the cell wall of the bacterial cells could form bidentate bridging complexes with the Eu^{III} metals. However, further studies would be needed, as there is no evidence of the frequency of the asymmetric $\nu(COO^-)$ mode. EXAFS analysis could provide more detailed information about the local coordination of Eu associated with these cells, but it falls beyond the main scope of this study. This would provide more unequivocal indications of the ability of bentonite-isolated bacteria to interact with Eu in a unidentate or

https://dx.doi.org/10.1021/acs.est.0c02418
Environ. Sci. Technol. 2020, 54, 15180−15190

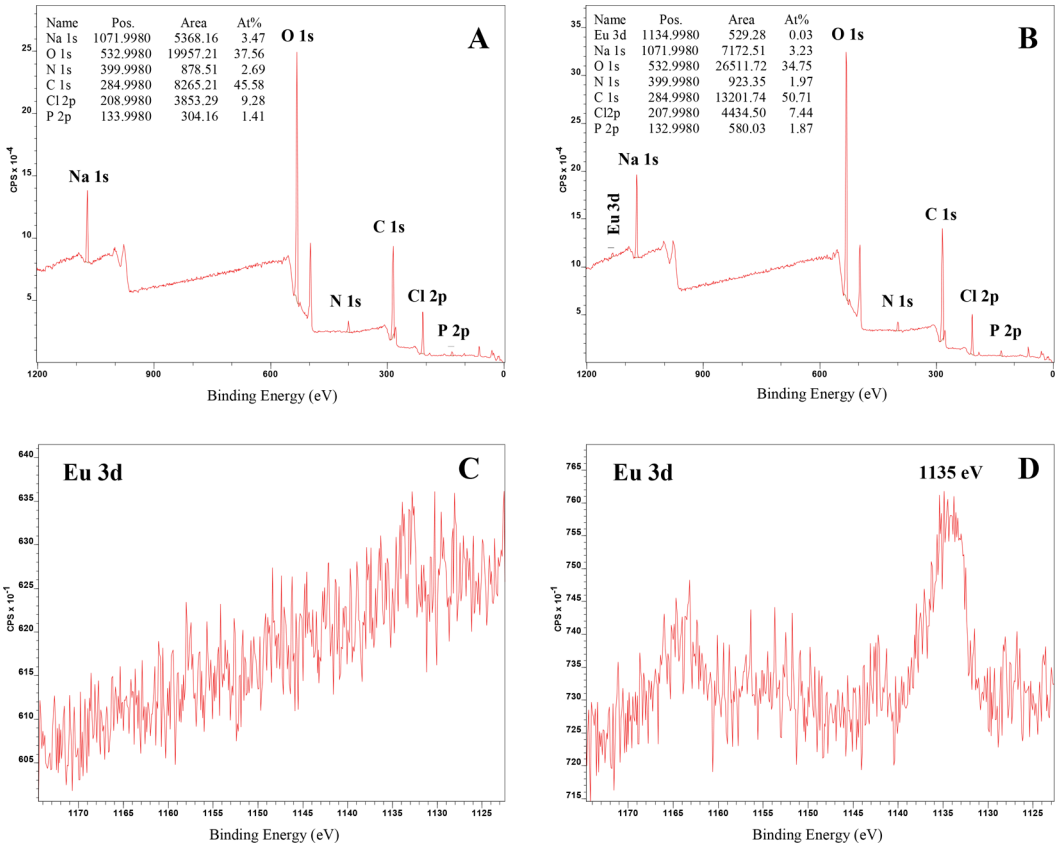

Figure 2. XPS spectra of *S. bentonitica* in absence (A, C) and presence of 30 μM Eu^{III} (B, D). High-resolution spectra of the region belonging to Eu 3d (C, D).

bidentate bridging mode. Nevertheless, these results provide further verification that carboxyl functional groups from the macromolecues of the bacterial cells are responsible in forming organometallic complexes with the Eu^{III} metals, as also reported by the potentiometric and luminiscence results.

In addition, the ATR-FTIR spectra indicated that phospholipids might also be involved in the cell−metal complexation. The lower intensity of the band found at 933 cm^{-1} of Eu^{III}-treated cells compared with Eu^{III}-untreated cells suggests phosphate groups as candidates for Eu^{III} complexation.[23]

3.4. Characterization of Eu^{III}–*S. bentonitica* Interactions Using XPS. This method was applied to determine the local coordination of Eu^{III} at the cell surface of *S. bentonitica* approximately up to 5 nm.[45] The elemental composition of the *S. bentonitica* surface, resulting from integrating the C_{1s}, O_{1s}, N_{1s}, and P_{2p} from the wide scan spectrum, can be seen in Figure 2A−D. Sodium and chlorine were also detected as samples were washed with 0.1 M $NaClO_4$. Eu was detected in the bacterial sample in contact with a 30 μM Eu^{III} solution for 48 h. Nitrogen appeared at a binding energy of 399.99 eV, attributable to amine or amide groups of proteins.[23,46−49] Phosphorus was found at a binding energy of 133.99 eV and can be attributed to phosphate groups.[47−49] The presence of amine groups from proteins and phosphate groups based on the binding energies of N_{1s} and P_{2p} are in agreement with the results from potentiometric titrations (pK_a = 6.8 and pK_a = 9.4) and the FTIR spectra (adsorption bands at 1635 cm^{-1}, 1535 cm^{-1}, and 933 cm^{-1}).

XPS peaks corresponding to Eu_{3d} were also analyzed at high resolution to assess the nature of the Eu^{III} complex and are shown in Figure 2D. The local coordination of Eu associated with the cells of the studied strain, observed at 1135 eV, is similar to that of Eu-acetate as was described by Mercier et al.[50] This suggests that carboxyl groups containing cell wall molecules such as glutamic acid of peptidoglycan are involved in the Eu binding. Previous studies showed the role of carboxyl groups from glutamic and aspartic acid present in proteins of the S-layer of *B. sphaericus* in the complexation of uranium and palladium.[51,52] Therefore, carboxyl groups of the glutamic acid of the peptidoglycan (PG) layer of *S. bentonitica* could be involved in the interaction of Eu^{III}.

3.5. TRLFS Characterization of Eu^{III}/Cm^{III} Interaction with *S. bentonitica*. Potentiometric titrations, ATR-FTIR, and XPS studies showed the involvement of phosphate and carboxyl groups in the coordination of Eu^{III} by the *S. bentonitica* cells. In addition, Eu^{III} and Cm^{III} were used as luminescence probes to investigate Cm^{III}/Eu^{III} binding on *S. bentonitica* based on changes of the intrinsic luminescence properties due to microbial interaction. The studies with Cm^{III}, radioactive analogue of Eu^{III}, were carried out at much lower concentrations relevant to environmental conditions (0.3 μM).

3.5.1. Europium. The luminescence spectra depicted in Figure 3 show the interaction of Eu^{III} with *S. bentonitica* through typical changes as result of cell addition after 1, 24, and 48 h of anaerobic incubation at pH 6 in both supernatants and resuspended cells. This suggested the complexation of Eu^{III} with extracellular released complexing agents and bacterial surface functional groups, respectively. In the supernatant and the resuspended cells the $^7F_0$ transition appeared at 579 nm with a slightly higher intensity than in the blank sample. This pointed to a different symmetry around the

https://dx.doi.org/10.1021/acs.est.0c02418
Environ. Sci. Technol. 2020, 54, 15180−15190

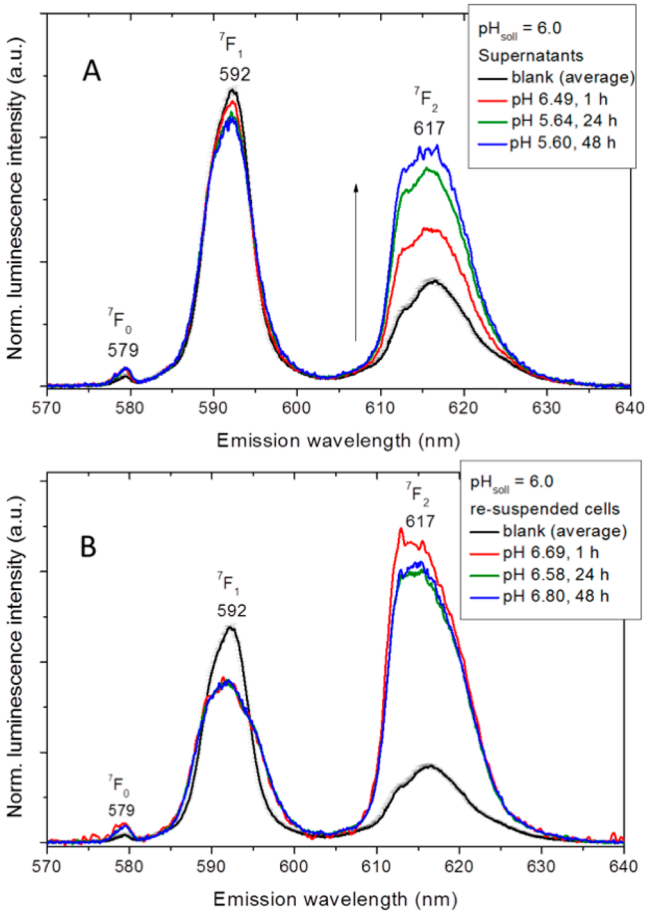

Figure 3. Luminescence emission spectra of 30 μM Eu^{III} measured for the supernatants after separating the *S. bentonitica* cells (0.2 g/L) (A) and the resuspended cells (B) under anaerobic conditions at pH 6 and different incubation times (1, 24, and 48 h) in 1 M $NaClO_4$.

Eu^{III} center compared to the blank spectrum and is a further argument for the interaction process of Eu^{III} with the cells. The luminescence spectrum of Eu^{III} aqua ion (blank) is characterized by emission bands at 585−600 nm (magnetic dipole transition $^5D_0 \rightarrow {}^7F_1$) and 610−630 nm (hypersensitive transition $^5D_0 \rightarrow {}^7F_2$). An increased intensity of the hypersensitive $^7F_2$ transition at 617 nm moving from blank via supernatant to the resuspended cells was discovered.

In the supernatants, there was a systematic increase in the $^7F_2$ transition as a function of the incubation time (Figure 3A). This could indicate an increase in the release of complexing agents from the cells at a longer incubation time. Total organic carbon (TOC) content of the supernatant samples increased after 24 h of incubation (Figure S3), suggesting the release of complexing substances from the cells. These results are in agreement with the Eu^{III} removal studies (section 3.2), in which the amount of Eu adsorbed increased with the incubation time. In the resuspended cells, there was a fast rise in the intensity of the $^7F_2$ transition after an incubation time of 1 h. Then no systematic changes in the spectra, as a function of the incubation time, were observed (Figure 3B).

In supernatants and resuspended cells, Eu^{III} appeared in two different coordination environments. The short-lived component in supernatants was measured at 117, 129, and 133 μs after 1, 24, and 48 h, respectively (Table 1). These lifetimes indicated a similar coordination environment after 24 and 48 h. Those Eu^{III} species containing approximately eight water molecules and one binding site will be filled by functionalities of the released substances. The luminescence lifetime of 114 ± 5 μs corresponding to 8.8 ± 0.5 coordinated water molecules found in the blank was characteristic to the Eu^{3+} ion. The short lifetime of 117 μs found in the supernatant after 1 h of incubation indicated the presence of the Eu^{III} ion. The longer lifetimes, 387 to 500 μs, could indicate an interaction of Eu^{III} with released substances from the cells independently from the incubation time. In this second type of Eu^{III} complex only up to one to two water molecules remained. In the case of resuspended cells, a biexponential luminescence decay was measured indicating two coordination environments of Eu^{III}. The short-lived component showed luminescence lifetimes between 144 and 225 μs (seven and four coordinated water molecules, respectively), whereas the long-lived component varied between 477 and 609 μs (two and one coordinated water molecules, respectively). In a first approximation, similar Eu^{III} species were formed for the short-lived component of the supernatant and resuspended cells. In the same way, the long-lived component of both supernatant and resuspended cells

Table 1. Spectroscopic Properties Obtained from the Eu^{III}−*S. bentonitica* System at pH 6 Using Different Incubation Times and Other Relevant Model Systems

sample	$R_{E/M}$	lifetime (μs)	proposed species	reference
Eu^{III} control	0.50 ± 0.05	114 ± 5	Eu^{3+}	this work
Eu^{III}−*S. bentonitica* in supernatant				this work
1 h incubation	0.9	117; 387	Eu^{3+}; phosphoryl sites	
24 h incubation	1.2	129; 490	carboxyl; phosphoryl	
48 h incubation	1.3	133; 500	carboxyl; phosphoryl	
Eu^{III}−*S. bentonitica* in cells				this work
1 h incubation	2.3	144; 477	carboxyl; phosphoryl sites	
24 h incubation	2.1	174; 561	carboxyl; phosphoryl	
48 h incubation	2.1	225; 609	carboxyl; phosphoryl	
Eu^{III}−*Sporomusa* sp. MT-2.99	3.3	170	R-COO-Eu^{2+}	Moll et al.[12]
	1.8	515	R-O-PO_3H-Eu^{2+}	
Eu^{III}−*Bacillus subtilis*		230	carboxyl sites	Markai et al.[54]
		730	phosphoryl sites	
Eu^{III}−*Pseudomonas aeruginosa*		98−254	carboxyl sites	Texier et al.[53]
		534−677	phosphoryl sites	

https://dx.doi.org/10.1021/acs.est.0c02418
Environ. Sci. Technol. 2020, 54, 15180−15190

suggested a similar coordination environment but different from the one found for the short-lived component.

By comparing our lifetime results with literature data, phosphoryl and carboxyl groups present on bacterial cell envelopes and bacterial released substances seem to play an important role in the Eu^{III} coordination sites characterized by, for instance, their individual luminescence lifetimes, probably in the form of R-O-PO_3-Eu^{2+} (R-O-PO_3H-Eu^{2+} under acidic pH conditions) and R-COO-Eu^{2+} as revealed by previous studies (Table 1).[12,53] Specifically, the Eu^{III}−*S. bentonitica* complexes seem to have properties similar to those of the surface species R-O-PO_3H-Eu^{2+} observed on cell envelopes of *Sporomusa* sp. MT-2.99 as revealed by the long lifetimes.[12] The coordination site characterized by short lifetimes seem to interact with Eu^{III} with properties similar to those of the surface species R-COO-Eu^{2+} observed on cell envelopes of *Sporomusa* sp. MT-2.99 and *P. fluorescence*.[12] It is important to note that the results presented here were very similar to those obtained aerobically and have comparable significance (Figure S4).

3.5.2. Curium. The chemical speciation of Cm^{III} with *S. bentonitica* cells was studied at trace (0.3 μM) Cm^{III} concentrations by TRLFS. These measurements were conducted assuming that the influence of the luminescence properties of the microbial Cm^{III} species dominates over the influence of soluble Cm^{III} species with, for instance, released complexing agents. The pH-dependent spectroscopic Cm^{III} speciation in the cell suspensions is shown in Figure 4.

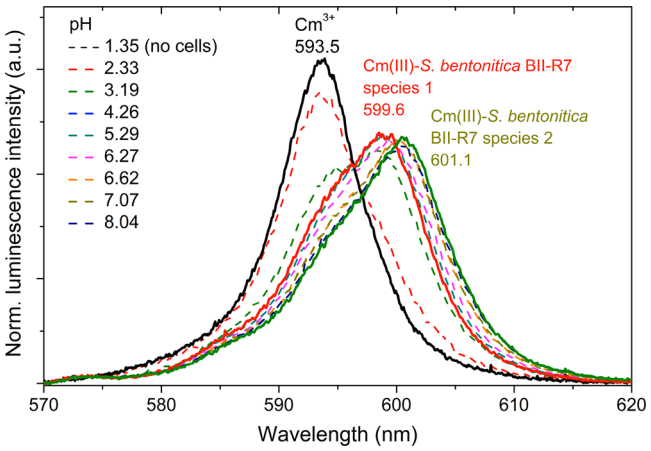

Figure 4. Luminescence emission spectra of 0.3 μM Cm^{III} in 0.1 M $NaClO_4$ measured as a function of pH at a fixed biomass concentration of 0.2 $g_{dry\ weight}$/L.

From the dependencies found in the TRLFS spectra, it can be concluded that there are two coordination environments of Cm^{III} due to interactions with functional groups of the cell surface and possibly with released complexing agents. Thus, the Hypspec analysis of the pH-dependent emission spectra measurements revealed two Cm^{III} bacterial species (Figure 4). Cm^{III}−*S. bentonitica* species 1 was characterized by an emission maximum at 599.6 nm while Cm^{III}−*S. bentonitica* species 2 showed a more red-shifted emission maximum at 601.1 nm. The extracted single component spectra of both species are shown in Figure 4. TRLFS of the supernatants and the Cm^{III}-loaded biomass after washing with 0.1 M $NaClO_4$ showed that 73% of the detected Cm^{III} luminescence intensity remained in solution at pH 8.04, while only 23% was associated with the biomass. This evidence indicated that a complexation of Cm^{III} by substances released from the cells was occurring. In all samples containing cells, a biexponential luminescence decay was detected (Table S3). At pH 3.2, the short lifetime of 71 μs points to uncomplexed Cm^{3+}. Between pH 4 and 8, both lifetimes amounted to 120 ± 8 and 290 ± 23 μs corresponding to five and two coordinated water molecules, respectively. By comparing our results with the ones reported in the literature, a close agreement was found to the study of Lopez-Fernandez et al.[15] The long lifetime and the corresponding emission maximum matches with Cm^{III} interactions with microbial phosphoryl sites, whereas the short lifetime can be attributed to carboxyl interactions of Cm^{III}.

3.6. Cellular Localization of Eu^{III} by STEM-HAADF (Scanning Transmission Electron Microscopy-High Angle Annular Dark Field). STEM-HAADF micrographs of thin sections of *S. bentonitica* cells exposed to Eu^{III} revealed the presence of electron-dense accumulations, mainly at the cell surface (Figure 5A−D) under both aerobic and anaerobic conditions. In addition, very few extracellular (Figure 5A−D) and intracellular (Figure 5D) accumulations were observed. EDX analysis (Figure 5E,F) and element-distribution mapping (Figure 6) of these accumulations indicated a main composition of Eu and P. The detection of P in the EDX analysis of the Eu^{III} precipitates also confirmed the key role of functional groups containing phosphorus in their interaction with Eu^{III}. These results showed biosorption of Eu^{III} as the main interaction mechanism with the cells of *S. bentonitica*. However, the presence of few extracellular and intracellular Eu^{III} precipitates indicated that the interaction is not only mediated by biosorption; thus, other processes, such as bioaccumulation and bioprecipitation, could also occur. This matches very well with the Eu^{III} removal studies (section 3.2) suggesting the implication of other interaction mechanisms.

The formation of outer membrane vesicles (OMVs) by *S. bentonitica cells* exposed to Eu^{III} was observed in the STEM-HAADF micrographs (Figure 5C,D). The production of OMVs by Gram-negative bacteria plays a prominent role in cell protection against hostile environments.[55,56] Morever, it represents a mechanism to alleviate stress through the packaging and release of stress-products.[57] Therefore, the vesicle formation mechanism of *S. bentonitica* cells could be involved in their Eu^{III} tolerance. In addition, the detection of extracellular precipitates could be a consequence of the release of intracellular accumulates through the formation of vesicles. However, further investigations are needed to confirm this hypothesis. On the other side, intracellullar accumulation could be a consequence of a passive process associated with damage of the cell membrane permeability, because Eu does not have any biological function and the cells do not have a specific transport system for the uptake of this element. The explanation of how and why elements such as Eu are accumulated in the cytoplasm of some microorganisms remains unknown.

3.7. Environmental Implications. The safety of the DGR system has been well studied from a geological, chemical, and physical point of view, but very few works have investigated the impact of microbial processes in the safety of this disposal option. It is well-known that microbes occurring in different DGR barriers, including bentonites, can affect the safety of a DGR through (1) corrosion of metal containers, (2) transformation and alteration of bentonite minerals, (3) gas production, and (4) mobilization of radionuclides present in

https://dx.doi.org/10.1021/acs.est.0c02418
Environ. Sci. Technol. 2020, 54, 15180−15190

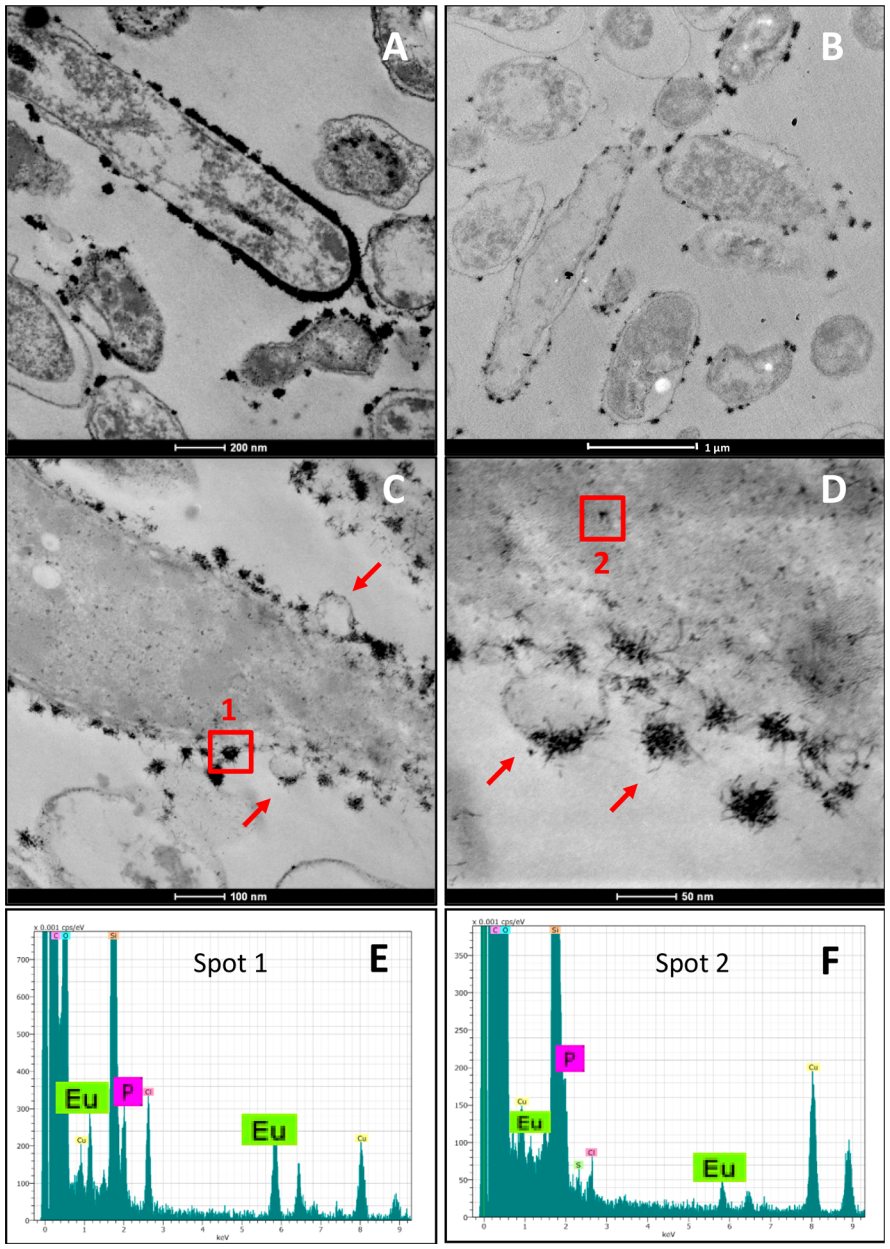

Figure 5. STEM-HAADF micrographs showing electron-dense accumulations at the cell surface, extracellularly, and intracellularly under aerobic (A, B) and anaerobic conditions (C, D). EDX analysis (E, F) confirming the Eu and P composition of the accumulations. The formation of vesicles by *S. bentonitica* cells is indicated by arrows (C, D). Scale bars: 200 nm (A), 1 μm (B), 100 nm (C), 50 nm (D).

the system, such as curium, selenium, or uranium. Here we reported a clear effect of the activity of the bentonite bacterial isolate *S. bentonitica*, on the speciation and mobility of trivalent actinides such as Cm^{III} and its inactive analogue Eu^{III}.

A multidisciplinary approach combining microscopy, spectroscopy, and potentiometric titration-based methods allowed us to provide new insights on the speciation of Cm and Eu associated with bacterial strains (isolated from one of the most important arificial barriers, bentonites, of future DGRs). The results obtained revealed that carboxyl and phosporyl groups from bacterial envelopes and other extracellularly released complexing agents seem to be involved in the interaction with Eu and Cm. Specifically, XPS analysis suggested that these carboxyl groups could arise from macromolecules located at the cell surface such as glutamic acids of the peptidoglycan layer, which could be involved in the complexation of Eu^{III}. In addition, ATR-FTIR suggested that the coordination of Eu^{III} with carboxyl groups from the bacterial cell wall can occur in a bidendate bridging mode. Finally, TEM analysis, in combination with the rest of the techniques, suggested that the Eu/Cm−bacteria interaction most probably occurs through several microbial processes such as biosorption, intracellular accumulation, and biomineralization. The results reported here clearly suggest that *S. bentonitica* can influence the speciation and hence mobility of Eu and Cm, affecting the safety of the DGR system.

Biosorption and bioaccumulation may enable metal removal from contaminated aqueous solutions through the immobilization of bacterial biomass to inert supports,[58] which are nowadays receiving attention for bioremediation purposes. The immobilization of microorganisms in minerals from bentonites and other materials through the formation of biofilms can lead

https://dx.doi.org/10.1021/acs.est.0c02418
Environ. Sci. Technol. 2020, 54, 15180−15190

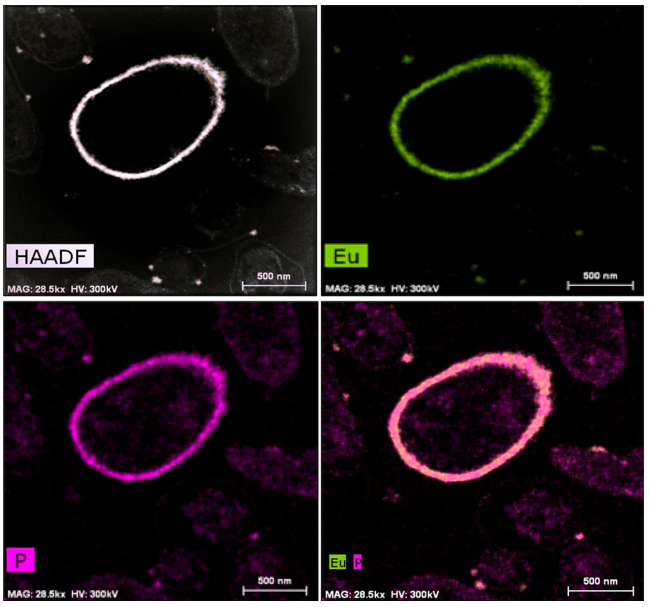

Figure 6. STEM-HAADF micrographs of thin sections showing the adsorption of Eu^{III} on a *S. bentonitica* cell after 48 h in contact with 30 μM Eu^{III} solution. Scale bars: 500 nm.

to the immobilization of bioadsorbed or bioaccumulated radionuclides. Indeed, genes coding for the formation of biofilms such as those involved in the formation of surface structures (*flhA*, *flhB*, *fliR*, *fliQ*, *fliP*, *fliN*, *fliM*)[59] or those encoding outer-membrane lipoproteins (*slp*)[60] have been reported to be present in the genome of *S. bentonitica*[61] (GenBank accession no. MKCZ00000000). In addition, the production of flagella-like proteins by this bacterium could be involved in the formation of biofilms. Clark et al.[62] demonstrated the role of flagella-like filaments produced by *Desulfovibrio vulgaris* in the establishment and maintenance of biofilms between cells and silica oxide surfaces. Therefore, *S. bentonitica* could positively influence the safety of repositories by inducing the immobilization of radionuclides through biofilm formation.

In addition to biosorption and bioaccumulation, a long-term bioprecipitation process could be involved as suggested by the extracellular Eu precipitates observed by STEM-HAADF. Bioprecipitation basically leads to the inmobilization of radionuclides because it is based on the conversion from soluble to insoluble forms through their precipitation with released cell ligands (carbonates, phosphates, etc.).[11,63] For all of the aforementioned reasons, the present study could be very helpful to better understand how microbes affect the safety of the disposal of radioactive residues, which is a global environmental concern nowadays.

■ ASSOCIATED CONTENT

Supporting Information

The Supporting Information is available free of charge at https://pubs.acs.org/doi/10.1021/acs.est.0c02418.

Five sections of methodology (1.1. Preparation of Eu^{III} and Cm^{III} stock solutions, 1.2. Potentiometric titration of cell surfaces of *S. bentonitica* treated with Eu^{III}, 1.3. Eu^{III} biosorption experiments, 1.4. TRLFS experimental setup, and 1.5. STEM-HAADF analysis), four figures, and three tables (PDF)

■ AUTHOR INFORMATION

Corresponding Authors

Miguel A. Ruiz-Fresneda − *Department of Microbiology, University of Granada, Granada, Spain;* orcid.org/0000-0001-6349-6566; Email: mafres@ugr.es

Margarita Lopez-Fernandez − *Helmholtz-Zentrum Dresden-Rossendorf, Institute of Resource Ecology, Dresden, Germany;* Email: margaritalopez@ugr.es

Authors

Marcos F. Martinez-Moreno − *Department of Microbiology, University of Granada, Granada, Spain*

Andrea Cherkouk − *Helmholtz-Zentrum Dresden-Rossendorf, Institute of Resource Ecology, Dresden, Germany;* orcid.org/0000-0002-3908-2539

Yon Ju-Nam − *Systems and Process Engineering Centre, College of Engineering, Swansea University, Swansea, U.K.*

Jesus J. Ojeda − *Systems and Process Engineering Centre, College of Engineering, Swansea University, Swansea, U.K.;* orcid.org/0000-0002-2046-1010

Henry Moll − *Helmholtz-Zentrum Dresden-Rossendorf, Institute of Resource Ecology, Dresden, Germany*

Mohamed L. Merroun − *Department of Microbiology, University of Granada, Granada, Spain*

Complete contact information is available at: https://pubs.acs.org/10.1021/acs.est.0c02418

Notes

The authors declare no competing financial interest.

■ ACKNOWLEDGMENTS

This work was supported by Euratom research and training programme 2014-2018 under grant agreement no. 661880 and ERDF-financed gants CGL-2012-36505, CGL2014-59616-R (80% funding by FEDER). Part of this work was cofinanced by the European Radioecology Alliance mobility grant awarded to MAR-F. The authors acknowledge the assistance of Maria del Mar Abad Ortega and Concepción Hernández Castillo (Centro de Instrumentación Cientifica, University of Granada, Spain) for their help with microscopy measurements, and Dr. James McGettrick (Swansea University, College of Engineering) for help with the XPS measurements. The authors are indebted to the U.S. Department of Energy, Office of Basic Energy Sciences, for the use of ^{248}Cm via the transplutonium element production facilities at Oak Ridge National Laboratory; ^{248}Cm was made available as part of a collaboration between HZDR and the Lawrence Berkeley National Laboratory (LBNL).

■ REFERENCES

(1) NEA. *Radioactive Waste in Perspective*; Nuclear Energy Agency: Paris, 2010. DOI: 10.1787/9789264092624-en.

(2) Stroes-Gascoyne, S.; Hamon, C. J.; Dixon, D. A.; Martino, J. B. Microbial Analysis of Samples from the Tunnel Sealing Experiment at AECL's Underground Research Laboratory. *Phys. Chem. Earth* **2007**, *32* (1−7), 219−231.

(3) Lopez-Fernandez, M.; Cherkouk, A.; Vilchez-Vargas, R.; Jauregui, R.; Pieper, D.; Boon, N.; Sanchez-Castro, I.; Merroun, M. L. Bacterial Diversity in Bentonites, Engineered Barrier for Deep Geological Disposal of Radioactive Wastes. *Microb. Ecol.* **2015**, *70* (4), 922−935.

(4) López-Fernández, M.; Fernández-Sanfrancisco, O.; Moreno-García, A.; Martín-Sánchez, I.; Sánchez-Castro, I.; Merroun, M. L.

Microbial Communities in Bentonite Formations and Their Interactions with Uranium. *Appl. Geochem.* **2014**, *49*, 77−86.
(5) Meleshyn, A. Microbial Processes Relevant for Long-Term Performance of Radioactive Waste Repositories in Clays. Gesellschaft für Anlagen-und Reaktorsicherheit (GRS) mbH. GRS − 291, 2011. Available from https://www.grs.de/sites/default/files/pdf/GRS-291.pdf.
(6) Newsome, L.; Morris, K.; Lloyd, J. R. The Biogeochemistry and Bioremediation of Uranium and Other Priority Radionuclides. *Chem. Geol.* **2014**, *363*, 164−184.
(7) Gorietti, D.; Giardina, I.; Arginelli, D.; Battisti, P. Determination of Plutonium, Americium and Curium Isotopes in Radioactive Metal Wastes Deriving from Nuclear Decommissioning. *J. Radioanal. Nucl. Chem.* **2017**, *314* (3), 1785−1792.
(8) Kooyman, T.; Buiron, L.; Rimpault, G. A Comparison of Curium, Neptunium and Americium Transmutation Feasibility. *Ann. Nucl. Energy* **2018**, *112*, 748−758.
(9) Edelstein, N. M.; Klenze, R.; Fanghänel, T.; Hubert, S. Optical Properties of Cm(III) in Crystals and Solutions and Their Application to Cm(III) Speciation. *Coord. Chem. Rev.* **2006**, *250* (7−8), 948−973.
(10) Ansoborlo, E.; Bion, L.; Doizi, D.; Moulin, C.; Lourenco, V.; Madic, C.; Cote, G.; Van der Lee, J.; Moulin, V. Current and Future Radionuclide Speciation Studies in Biological Media. *Radiat. Prot. Dosim.* **2007**, *127* (1−4), 97−102.
(11) Shukla, A.; Parmar, P.; Saraf, M. Radiation, Radionuclides and Bacteria: An in-Perspective Review. *J. Environ. Radioact.* **2017**, *180* (11), 27−35.
(12) Moll, H.; Lütke, L.; Bachvarova, V.; Cherkouk, A.; Selenska-Pobell, S.; Bernhard, G. Interactions of the Mont Terri Opalinus Clay Isolate *Sporomusa* sp. MT-2.99 with Curium(III) and Europium(III). *Geomicrobiol. J.* **2014**, *31* (8), 682−696.
(13) Reitz, T.; Rossberg, A.; Barkleit, A.; Steudtner, R.; Selenska-Pobell, S.; Merroun, M. L. Spectroscopic Study on Uranyl Carboxylate Complexes Formed at the Surface Layer of *Sulfolobus acidocaldarius*. *Dalt. Trans.* **2015**, *44* (6), 2684−2692.
(14) Moll, H.; Lütke, L.; Barkleit, A.; Bernhard, G. Curium(III) Speciation Studies with Cells of a Groundwater Strain of *Pseudomonas fluorescens*. *Geomicrobiol. J.* **2013**, *30* (4), 337−346.
(15) Lopez-Fernandez, M.; Moll, H.; Merroun, M. L. Reversible pH-Dependent Curium(III) Biosorption by the Bentonite Yeast Isolate *Rhodotorula mucilaginosa* BII-R8. *J. Hazard. Mater.* **2019**, *370*, 156−163.
(16) Bader, M.; Moll, H.; Steudtner, R.; Lösch, H.; Drobot, B.; Stumpf, T.; Cherkouk, A. Association of Eu(III) and Cm(III) onto an Extremely Halophilic Archaeon. *Environ. Sci. Pollut. Res.* **2019**, *26* (9), 9352−9364.
(17) Ojeda, J. J.; Romero-González, M. E.; Bachmann, R. T.; Edyvean, R. G. J.; Banwart, S. A. Characterization of the Cell Surface and Cell Wall Chemistry of Drinking Water Bacteria by Combining XPS, FTIR Spectroscopy, Modeling, and Potentiometric Titrations. *Langmuir* **2008**, *24* (8), 4032−4040.
(18) Fein, J. B.; Boily, J. F.; Yee, N.; Gorman-Lewis, D.; Turner, B. F. Potentiometric Titrations of Bacillus Subtilis Cells to Low pH and a Comparison of Modeling Approaches. *Geochim. Cosmochim. Acta* **2005**, *69* (5), 1123−1132.
(19) Krawczyk-Bärsch, E.; Gerber, U.; Müller, K.; Moll, H.; Rossberg, A.; Steudtner, R.; Merroun, M. L. Multidisciplinary Characterization of U(VI) Sequestration by *Acidovorax facilis* for Bioremediation Purposes. *J. Hazard. Mater.* **2018**, *347*, 233−241.
(20) Villar, M. V.; Pérez del Villar, L.; Martín, P. L.; Pelayo, M.; Fernández, A. M.; Garralón, A.; Cuevas, J.; Leguey, S.; Caballero, E.; Huertas, F. J.; Jiménez de Cisneros, C.; Linares, J.; Reyes, E.; Delgado, A.; Fernández-Soler, J. M.; Astudillo, J. The Study of Spanish Clays for Their Use as Sealing Materials in Nuclear Waste Repositories: 20 Years of Progress. *J. Iber. Geol.* **2006**, *32* (1), 15−36.
(21) Ruiz Fresneda, M. A.; Delgado Martín, J.; Gómez Bolívar, J.; Fernández Cantos, M. V.; Bosch-Estévez, G.; Martínez Moreno, M. F.; Merroun, M. L. Green Synthesis and Biotransformation of Amorphous Se Nanospheres to Trigonal 1D Se Nanostructures: Impact on Se Mobility within the Concept of Radioactive Waste Disposal. *Environ. Sci.: Nano* **2018**, *5* (9), 2103−2116.
(22) Sánchez-Castro, I.; Ruiz-Fresneda, M. A.; Bakkali, M.; Kämpfer, P.; Glaeser, S. P.; Busse, H. J.; López-Fernández, M.; Martínez-Rodríguez, P.; Merroun, M. L. *Stenotrophomonas bentonitica* sp. nov., Isolated from Bentonite Formations. *Int. J. Syst. Evol. Microbiol.* **2017**, *67* (8), 2779−2786.
(23) Omoike, A.; Chorover, J. Spectroscopic Study of Extracellular Polymeric Substances from *Bacillus subtilis*: Aqueous Chemistry and Adsorption Effects. *Biomacromolecules* **2004**, *5* (4), 1219−1230.
(24) Fairley, N. CasaXPS 2.3.17 ed.; Casa Software Ltd., 2006. Available from www.casaxps.com.
(25) Fein, J. B.; Daughney, C. J.; Yee, N.; Davis, T. A. A Chemical Equilibrium Model for Metal Adsorption onto Bacterial Surfaces. *Geochim. Cosmochim. Acta* **1997**, *61* (16), 3319−3328.
(26) Turner, B. F.; Fein, J. B. Protofit: A Program for Determining Surface Protonation Constants from Titration Data. *Comput. Geosci.* **2006**, *32* (9), 1344−1356.
(27) Borrok, D. M.; Fein, J. B. The Impact of Ionic Strength on the Adsorption of Protons, Pb, Cd, and Sr onto the Surfaces of Gram Negative Bacteria: Testing Non-Electrostatic, Diffuse, and Triple-Layer Models. *J. Colloid Interface Sci.* **2005**, *286*, 110.
(28) Borrok, D.; Turner, B. F.; Fein, J. B. A Universal Surface Complexation Framework for Modeling Proton Binding onto Bacterial Surfaces in Geologic Settings. *Am. J. Sci.* **2005**. *305826*.
(29) Ngwenya, B. T.; Sutherland, I. W.; Kennedy, L. Comparison of the Acid-Base Behaviour and Metal Adsorption Characteristics of a Gram-Negative Bacterium with Other Strains. *Appl. Geochem.* **2003**, *18* (4), 527−538.
(30) Dittrich, M.; Sibler, S. Cell Surface Groups of Two Picocyanobacteria Strains Studied by Zeta Potential Investigations, Potentiometric Titration, and Infrared Spectroscopy. *J. Colloid Interface Sci.* **2005**, *286* (2), 487−495.
(31) Yee, N.; Benning, L. G.; Phoenix, V. R.; Ferris, F. G. Characterization of Metal-Cyanobacteria Sorption Reactions: A Combined Macroscopic and Infrared Spectroscopic Investigation. *Environ. Sci. Technol.* **2004**, *38* (3), 775−782.
(32) Yee, N.; Fein, J. Cd Adsorption onto Bacterial Surfaces: A Universal Adsorption Edge? *Geochim. Cosmochim. Acta* **2001**, *65* (13), 2037−2042.
(33) Claessens, J.; van Lith, Y.; Laverman, A. M.; Van Cappellen, P. Acid-Base Activity of Live Bacteria: Implications for Quantifying Cell Wall Charge. *Geochim. Cosmochim. Acta* **2006**, *70* (2), 267−276.
(34) Merroun, M. L.; Nedelkova, M.; Ojeda, J. J.; Reitz, T.; Fernández, M. L.; Arias, J. M.; Romero-González, M.; Selenska-Pobell, S. Bio-Precipitation of Uranium by Two Bacterial Isolates Recovered from Extreme Environments as Estimated by Potentiometric Titration, TEM and X-Ray Absorption Spectroscopic Analyses. *J. Hazard. Mater.* **2011**, *197*, 1−10.
(35) Fang, L.; Yang, S.; Huang, Q.; Xue, A.; Cai, P. Biosorption Mechanisms of Cu(II) by Extracellular Polymeric Substances from *Bacillus subtilis*. *Chem. Geol.* **2014**, *386*, 143−151.
(36) Liu, Y.; Alessi, D. S.; Owttrim, G. W.; Petrash, D. A.; Mloszewska, A. M.; Lalonde, S. V.; Martinez, R. E.; Zhou, Q.; Konhauser, K. O. Cell Surface Reactivity of *Synechococcus* sp. PCC 7002: Implications for Metal Sorption from Seawater. *Geochim. Cosmochim. Acta* **2015**, *169*, 30−44.
(37) Ozaki, T.; Gillow, J. B.; Kimura, T.; Ohnuki, T.; Yoshida, Z.; Francis, A. J. Sorption Behavior of Europium(III) and Curium(III) on the Cell Surfaces of Microorganisms. *Radiochim. Acta* **2004**, *92* (9−11), 741−748.
(38) Yao, T.; Wu, X.; Chen, X.; Xiao, Y.; Zhang, Y.; Zhao, Y.; Li, F. Biosorption of Eu(III) and U(VI) on *Bacillus subtilis*: Macroscopic and Modeling Investigation. *J. Mol. Liq.* **2016**, *219*, 32−38.
(39) Gadd, G. M. Biosorption: Critical Review of Scientific Rationale, Environmental Importance and Significance for Pollution Treatment. *J. Chem. Technol. Biotechnol.* **2009**, *84* (1), 13−28.
(40) Jiang, W.; Saxena, A.; Song, B.; Ward, B. B.; Beveridge, T. J.; Myneni, S. C. B. Elucidation of Functional Groups on Gram-Positive

https://dx.doi.org/10.1021/acs.est.0c02418
Environ. Sci. Technol. 2020, 54, 15180−15190

and Gram-Negative Bacterial Surfaces Using Infrared Spectroscopy. *Langmuir* **2004**, *20* (26), 11433−11442.
(41) Chu, H. A.; Hillier, W.; Debus, R. J. Evidence That the C-Terminus of the D1 Polypeptide of Photosystem II Is Ligated to the Manganese Ion That Undergoes Oxidation during the S1 to S2 Transition: An Isotope-Edited FTIR Study. *Biochemistry* **2004**, *43* (11), 3152−3166.
(42) Nakamoto, K. *Infrared and Raman Spectra of Inorganic and Coordination Compounds: Part B: Applications in Coordination, Organometallic, and Bioinorganic Chemistry*, 6th ed.; Wiley: Hoboken, NJ, 2008. DOI: 10.1002/9780470405888.
(43) Tackett, J. E. FT-IR Characterization of Metal Acetates in Aqueous Solution. *Appl. Spectrosc.* **1989**, *43* (3), 483−489.
(44) Deacon, G. B.; Phillips, R. J. Relationships between the Carbon-Oxygen Stretching Frequencies of Carboxylato Complexes and the Type of Carboxylate Coordination. *Coord. Chem. Rev.* **1980**, *33* (3), 227−250.
(45) Kumar, S.; Prakash, R.; Singh, V. Synthesis, Characterization, and Applications of Europium Oxide: A Review. *Rev. Adv. Sci. Eng.* **2015**, *4* (4), 247−257.
(46) Pradier, C. M.; Rubio, C.; Poleunis, C.; Bertrand, P.; Marcus, P.; Compère, C. Surface Characterization of Three Marine Bacterial Strains by Fourier Transform IR, X-Ray Photoelectron Spectroscopy, and Time-of-Flight Secondary-Ion Mass Spectrometry, Correlation with Adhesion on Stainless Steel Surfaces. *J. Phys. Chem. B* **2005**, *109* (19), 9540−9549.
(47) Van Der Mei, H. C.; De Vries, J.; Busscher, H. J. X-Ray Photoelectron Spectroscopy for the Study of Microbial Cell Surfaces. *Surf. Sci. Rep.* **2000**, *39* (1), 1−24.
(48) Dufrêne, Y. F.; Van der Wal, A.; Norde, W.; Rouxhet, P. G. X-Ray Photoelectron Spectroscopy Analysis of Whole Cells and Isolated Cell Walls of Gram-Positive Bacteria: Comparison with Biochemical Analysis. *J. Bacteriol.* **1997**, *179* (4), 1023−1028.
(49) Dufrêne, Y. F.; Rouxhet, P. G. X-Ray Photoelectron Spectroscopy Analysis of the Surface Composition of *Azospirillum brasilense* in Relation to Growth Conditions. *Colloids Surf., B* **1996**, *7* (5−6), 271−279.
(50) Mercier, F.; Alliot, C.; Bion, L.; Thromat, N.; Toulhoat, P. XPS Study of Eu(III) Coordination Compounds: Core Levels Binding Energies in Solid Mixed-Oxo-Compounds EumXxOy. *J. Electron Spectrosc. Relat. Phenom.* **2006**, *150* (1), 21−26.
(51) Merroun, M. L.; Raff, J.; Rossberg, A.; Hennig, C.; Reich, T.; Selenska-Pobell, S. Complexation of Uranium by Cells and S-Layer Sheets of *Bacillus sphaericus* JG-A12. *Appl. Environ. Microbiol.* **2005**, *71* (9), 5532−5543.
(52) Fahmy, K.; Merroun, M.; Pollmann, K.; Raff, J.; Savchuk, O.; Hennig, C.; Selenska-Pobell, S. Secondary Structure and Pd(II) Coordination in S-Layer Proteins from *Bacillus sphaericus* Studied by Infrared and X-Ray Absorption Spectroscopy. *Biophys. J.* **2006**, *91* (3), 996−1007.
(53) Texier, A. C.; Andrés, Y.; Illemassene, M.; Le Cloirec, P. Characterization of Lanthanide Ions Binding Sites in the Cell Wall of *Pseudomonas aeruginosa*. *Environ. Sci. Technol.* **2000**, *34* (4), 610−615.
(54) Markai, S.; Andrès, Y.; Montavon, G.; Grambow, B. Study of the Interaction between Europium (III) and *Bacillus subtilis*: Fixation Sites, Biosorption Modeling and Reversibility. *J. Colloid Interface Sci.* **2003**, *262* (2), 351−361.
(55) Toyofuku, M.; Nomura, N.; Eberl, L. Types and Origins of Bacterial Membrane Vesicles. *Nat. Rev. Microbiol.* **2019**, *17*, 13−24.
(56) Jan, A. T. Outer Membrane Vesicles (OMVs) of Gram-Negative Bacteria: A Perspective Update. *Front. Microbiol.* **2017**, *8*, 1053.
(57) Klimentová, J.; Stulík, J. Methods of Isolation and Purification of Outer Membrane Vesicles from Gram-Negative Bacteria. *Microbiol. Res.* **2015**, *170*, 1−9.
(58) Gadd, G. M. Microbial Influence on Metal Mobility and Application for Bioremediation. *Geoderma* **2004**, *122* (2−4), 109−119.
(59) Niba, E. T. E.; Naka, Y.; Nagase, M.; Mori, H.; Kitakawa, M. A Genome-Wide Approach to Identify the Genes Involved in Biofilm Formation in *E. coli*. *DNA Res.* **2008**, *14* (6), 237−246.
(60) Prigent-Combaret, C.; Vidal, O.; Dorel, C.; Lejeune, P. Abiotic Surface Sensing and Biofilm-Dependent Regulation of Gene Expression in Escherichia Coli. *J. Bacteriol.* **1999**, *181* (19), 5993−6002.
(61) Sánchez-Castro, I.; Bakkali, M.; Merroun, M. L. Draft Genome Sequence of *Stenotrophomonas bentonitica* BII-R7, a Selenite-Reducing Bacterium Isolated from Spanish Bentonites. *Genome Announc.* **2017**, *5* (31), e00719-17. DOI: 10.1128/genomeA.00719-17.
(62) Clark, M. E.; Edelmann, R. E.; Duley, M. L.; Wall, J. D.; Fields, M. W. Biofilm Formation in *Desulfovibrio vulgaris* Hildenborough Is Dependent upon Protein Filaments. *Environ. Microbiol.* **2007**, *9* (11), 2844−2854. DOI: 10.1111/j.1462-2920.2007.01398.x.
(63) Rui, X.; Kwon, M. J.; O'Loughlin, E. J.; Dunham-Cheatham, S.; Fein, J. B.; Bunker, B.; Kemner, K. M.; Boyanov, M. I. Bioreduction of Hydrogen Uranyl Phosphate: Mechanisms and U(IV) Products. *Environ. Sci. Technol.* **2013**, *47* (11), 5668−5678.